Economic Geology
Vol. 82, 1987, pp. 1319–1333

Geology of Skarn and High-Grade Gold in the Carr Fork Mine, Utah

DONALD E. CAMERON

P.O. Box 250, Rico, Colorado 81332

AND W. J. GARMOE

2371 Cavalier Drive, Salt Lake City, Utah 84121

Abstract

High-grade gold mineralization occurs as an overprint to copper-gold skarns in the Carr Fork mine. Geological and geochemical studies and geostatistical comparison of the distribution of gold in the copper-gold skarns and in the high-grade gold mineralization show that gold was deposited in two separate and distinguishable events: deposition with copper in skarn ores, under multiple controls, and high-grade gold mineralization, which formed a shoot in skarns hosted by the Parnell limestone. The gold content of material produced at this stage is much higher than that of the skarn ores.

High-grade gold accompanies distinct alteration characterized by clay pyrite and quartz-pyrite(-tennantite), anomalous Au, As, Sb, Hg, Si, S, and Tl, and depletion of Pd, Ca, and Se. The high-grade gold mineralization comprises at least three episodes determined from petrographic and microprobe studies; it preceded the quartz molybdenum veins.

The statistical characteristics of the high-grade gold are separable from the copper-gold mineralization in histograms, scattergrams, and variograms. The mean of the high-grade gold composites is 0.3 troy oz/short ton. Directional variograms of skarn ore show that a pervasive N 20° E fault set and the distance to the Bingham stock contact controlled the copper and gold grades. Elevation seems to have been an additional control on gold grades in skarn.

The shoot of high-grade gold mineralization in the Parnell limestone comprises a diluted drilled resource of 1.2 million tons. Evidence suggests that it continues some distance beyond present drilling.

Introduction

THE Carr Fork mine is located in the Bingham mining district 9 km east of Tooele, Utah. The mine is immediately west of, and adjacent to, the Utah Copper open-pit mine. The Carr Fork orebodies are continuous with skarn ores in limestones in the contact aureole of the Bingham stock. These were exploited in the Utah Apex mine prior to 1947. The top of the orebodies was a residual gold-enriched capping, which gave way in depth to supergene copper-gold sulfide ores, and finally to hypogene sulfide replacement ores (cf. Boutwell, 1905, p. 85 and 265).

Hansen (1961, p. 70) listed the composite total production of lead, copper, silver, and gold from the copper skarn, copper-lead-zinc, and lead-zinc-silver orebodies of Carr Fork prior to 1947. Most of the production was from the Highland Boy, Yampa, and Parnell limestone beds.

From August 1979 to November 1981, the Carr Fork mine produced concentrates from copper-gold-silver skarn ores from a reserve estimated to be 61 million metric tons, averaging 1.89 percent copper, 0.027 percent molybdenum, 0.011 troy oz/ton gold, and 0.311 troy oz/ton silver. Molybdenum was not recovered in the Carr Fork mill. The metal production from the mine is presented in Table 1.

The high-grade gold resource described in this paper was being drilled at the time of shutdown, but there has been no production from it. At present, the mine is flooded. However, the resource and its potential extensions may someday be considered an attractive target for exploration in the Carr Fork mine, and similar mineralization may possibly occur in other parts of the Bingham district.

Geologic Setting of the Mine

Atkinson and Einaudi (1978) ably described many aspects of the skarn geology in their comprehensive paper. The skarn ores occur in limestone units of the Bingham Mine Formation of Late Pennsylvanian age, a marine shelf facies. The stratigraphic section in the Carr Fork mine is shown in Figure 1. To the right of the section are shown the unit names used in mine mapping and by Atkinson and Einaudi (1978). On the left are shown the names of units mapped in surface outcrop and also shown in sections by Hansen (1961, fig. 14) and Hunt (1924). The correlation of surface units with the mine section is ours. It differs from the correlation accepted by Atkinson and Einaudi (1978). The main evidence for the proposed new correlations consists of the following points:

1. The detailed mine section in the Yampa-Lark-Highland Boy interval (Fig. 1, right side, mine usage) is a nearly perfect match with the Parnell-Yampa in-

0361-0128/87/711/1319-15$2.50

TABLE 1. Carr Fork Mine Production Summary

	1979	1980	1981	Total
Copper (lbs)	684,655	14,718,024	35,981,031	51,383,031
Silver (oz)	17,277	160,371	389,568	567,216
Gold (oz)	1,188	10,351	28,178	39,717

terval (Fig. 1, left side) as presented by Hansen (1961, fig. 14); the section is also described by Rubright and Hart (1968, p. 891).

2. The "South Bed," locally present in the mine workings, probably correlates with the Highland Boy limestone as mapped on the exposed surface and followed by mining in the Highland Boy mine.

3. Pre-1947 Yampa stopes (cf. Atkinson and Einaudi, 1978, p. 1327) of the Utah Apex mine immediately overlie Highland Boy stopes of the Carr Fork mine.

Thin limestones and distinctive interbedded bullseye-textured calcareous hornfels in the mine section match the descriptions of the interval encompassing the Rattlesnake and Bullseye limestones above the Yampa limestone bed in the section described by Hansen (1961). The Bullard limestone is in the same position relative to the Parnell and Yampa limestone beds (Fig. 1, left side) as is the Lark limestone to the Yampa and Highland Boy (Fig. 1, right side, mine usage) limestones.

The South Bed (A. Paul, unpub. rept., 1979) limestone intersects a mine working 160 m east of the B-B fault on the 1,200-m level of the mine (e.g., Fig. 2); it is intersected in several drill holes above the level. The footwall of the bed was intruded by Bingham monzonite, but even so the bed has a thickness of 12 to 15 m. The Highland boy limestone (mine usage) in this area can be followed upward to its intersection with the 1,300-m level of the mine. Old Yampa orebody stopes immediately overlie and certainly are continuous with Highland Boy (mine usage) orebody stopes, separated only by a crown pillar. The South Bed thus appears to correlate with the Highland Boy limestone bed mapped at surface and in the old workings; the Highland Boy limestone in mine usage (Fig. 1, right side) is the same as the Yampa limestone bed (Fig. 1, left side), and the Yampa limestone in mine usage (Fig. 1, right side) is the same as the Parnell limestone bed (Fig. 1, left side).

The proposed new correlations and terminology shown in Figure 1 (left side) are used in subsequent diagrams and in the rest of the paper. The new terminology is consistent with some of the published information on the near-surface skarns. However, most writers on the Bingham district, except for Emmons (1905) and Keith (1905), have reasonably assumed that the Yampa and Highland Boy limestones correlate with the Commercial and Jordan limestones, located on the east contact of the Bingham stock (Lark section). In fact, the Parnell, Bullard, and Yampa limestones probably correlate with the Commercial, Lark, and Jordan limestones described by Rubright and Hart (1968). The evidence for this is from deep drilling along the north edge of the stock by Kennecott Corporation's Utah Copper Division adjacent to the Carr Fork mine drilling. Here, the Parnell, Bullard, and Yampa limestones of the Carr Fork mine project into the Commercial, Lark, and Jordan limestones as encountered in Utah Copper drill holes.

The sedimentary rock sequence is folded into the Bingham anticline (Apex fold) and syncline whose common limb is locally overturned. These folds are similar folds and are marked by local extreme attenuation or thickening in fold limbs or troughs. The axial trace of the Bingham syncline in plan is shown in the geologic map (Fig. 2). The syncline is more easily visualized in the perspective drawing (Fig. 3). Intrusion of (quartz) monzonite of the mid-Tertiary Bingham stock truncated the nose of the structure. The northwest-trending Markham reverse fault offsets the north limb of the Bingham syncline and displaces the limestones approximately 380 m to the west in the hanging wall. The structure is mineralized and thus predates mineralization, but it was subsequently reactivated.

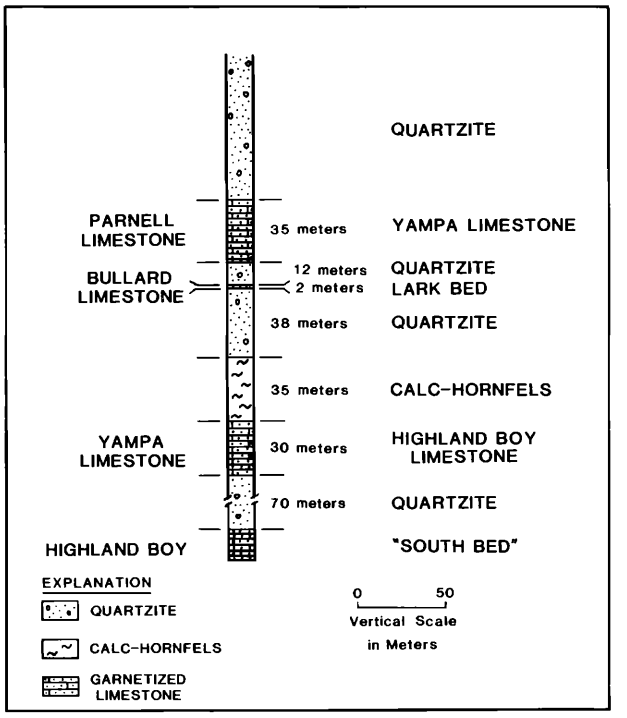

FIG. 1. Generalized stratigraphic section of the Carr Fork mine with old terminology (right side) compared to the proposed new correlations (left side).

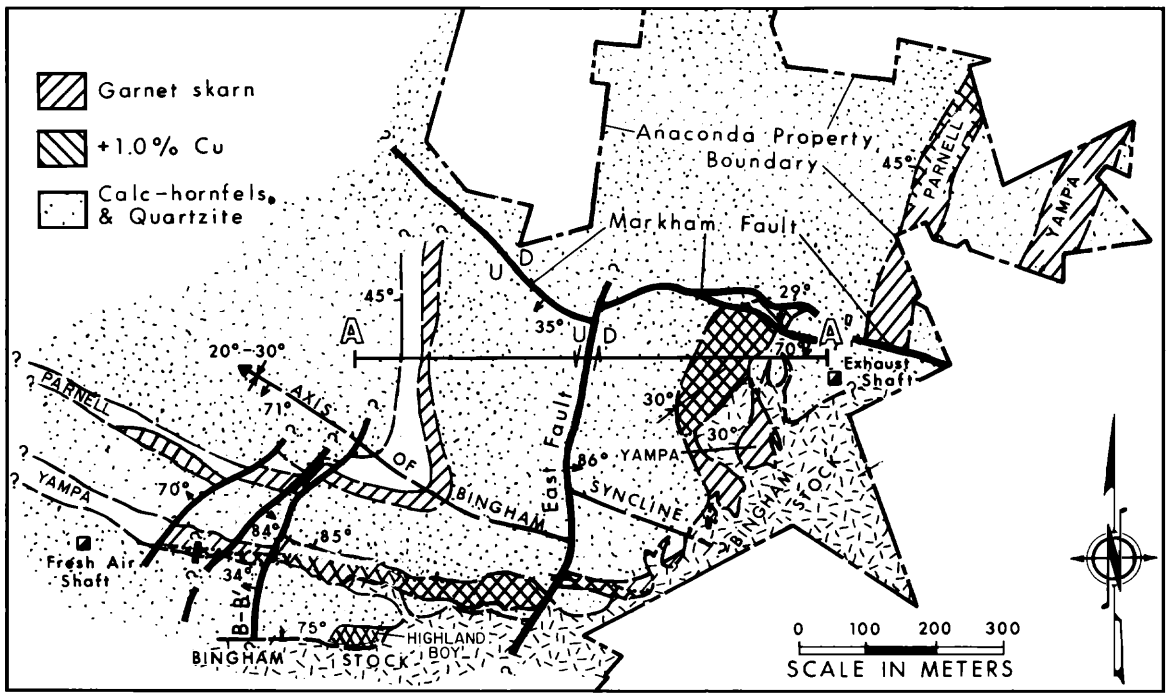

FIG. 2. Geologic map of the 1,200-m level of the Carr Fork mine showing distribution of garnet, skarn, and copper-gold mineralization.

The limestones are broken by innumerable minor faults, the most prominent of which form a set of northeast-striking and steeply dipping normal faults. The faults bend from northeast to north-northeast in strike as they cross the Bingham syncline axis. The East fault is the most significant of the northeast-striking faults (cf. Fig. 2). It has both left-lateral and normal displacement. The northeast fault set resulted in small step-wise or horst-graben offsets of small apparent displacement. Thus the dip of the limestones shown in section A-A' (Fig. 4) is net (apparent) dip and not the true local (apparent) dip of the beds. The northeast fault set is locally mineralized and probably provided the necessary ground preparation and access for mineralizing fluids, with contributions from northwest-striking and bedding plane structures.

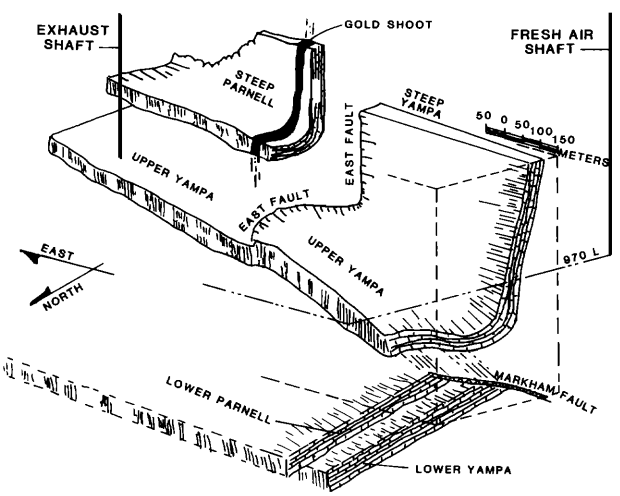

FIG. 3. Perspective view of the Carr Fork orebodies and the gold shoot looking southeast.

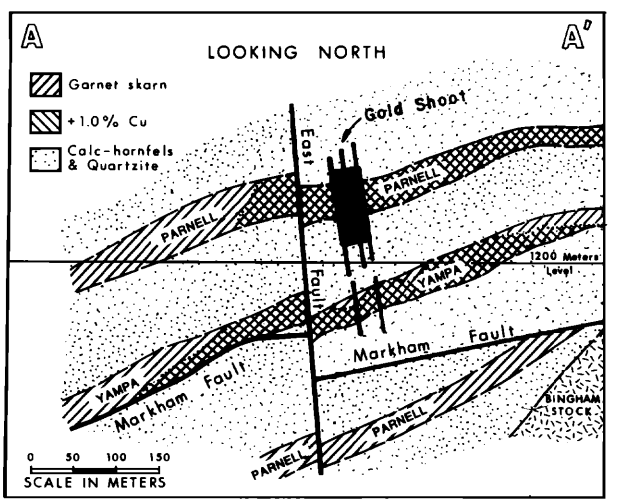

FIG. 4. Section A-A' across the north limb of the Bingham syncline showing the Parnell gold shoot.

The limestones are extensively altered to calc-silicate skarn assemblages in the mine area. Zonation of skarn minerals shown schematically in Figure 5 reflects both Early and Main Stage alteration episodes (cf. Atkinson and Einaudi, 1978, p. 1335–1351); thus not all the minerals in each zone formed contemporaneously. For example, diopside is generally present as relict patches or discontinuous layers veined by garnet and may have formed during magnesium and silica metasomatism of the Early Stage. Wollastonite, presumably formed by recrystallization of cherty limestone, may have preceded the Early Stage. Garnet, formed during iron and silica metasomatism of the Main Stage, appears to have overprinted the Early Stage diopside zone, and locally, the wollastonite zone. The result is that garnetite is locally in contact with black limestone. This alteration sequence with respect to the formation of diopside and garnet seems consistent with observed textural relationships in mine exposures and the alteration sequence for the silty limestones and quartzites hypothesized by Atkinson and Einaudi (1978).

Our proposed alteration sequence for the major limestone differs somewhat from that proposed by the Atkinson and Einaudi (1978). They state that diopside and garnet formed together as part of the Main Stage alteration. However, diopside apparently formed during the Early Stage magnesium metasomatism in silty limestones and quartzites; it seems logical, especially from the textural evidence presented above that diopside was a product of magnesium metasomatism in the major limestones as well.

Copper-Gold Orebodies

General description

The areas of ore with 1.0 percent copper in the limestones are shown on the 1,200-m level plan (Fig. 2) and the cross section (Fig. 4). The orebodies are named according to their positions with respect to the Markham fault, the axis of the Bingham syncline and the limestone bed by which they are hosted, e.g., the Lower Yampa and Upper Yampa orebodies lie northeast of the syncline axis and in the footwall and hanging wall of the Markham fault, respectively (cf. Figs. 2, 3, and 4). The Steep Yampa orebody lies southwest of the syncline axis. The Upper, Lower, and Steep Yampa orebodies are hosted by the Yampa limestone bed.

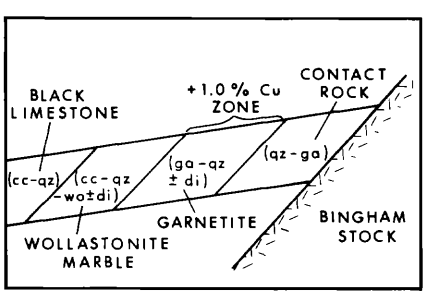

FIG. 5. Schematic diagram depicting alteration zones in the major limestones and their relation to the Bingham stock contact; cc = calcite, di = diopside, ga = garnet, qz = quartz, wo = wollastonite.

Mean whole-bed grade of mineralized rock in the garnetized Yampa and Parnell limestones is related to distance from the quartz monzonite porphyry unit of the Bingham stock (e.g., Atkinson and Einaudi, 1978, fig. 16). Mineralization was strongest in the lower third to half of the beds and in a narrow band at the hanging wall. Figure 6 depicts the distribution of copper across the Upper Parnell orebody in a characteristic drill hole. At the distal edges of the orebodies, 1.0 percent copper mineralization occurs only in the lower parts.

Chalcopyrite is the principal copper mineral present; it is closely associated with pyrite, and to a lesser degree, magnetite. These minerals occur as disseminations, vein fillings, closely spaced stringers, and bedding streaks. In detail the grade of mineralized rock is erratic and textures in ore samples commonly indicate multiple generations of chalcopyrite deposition. Molybdenite occurs in quartz veins which crosscut the copper-mineralized rock.

Gold is extremely fine grained and presumably occurs mostly as inclusions in the sulfide minerals. Much of the gold was recovered in the chalcopyrite concentrate produced by the flotation mill. Visible gold was observed in a single short interval of drill core.

Statistical and spatial distribution of copper and gold

Univariate statistics show that copper and gold have similar distributions; bivariate statistics show that copper and gold are highly correlated in the Carr Fork orebodies. The data base for the lower orebodies comprises seven existing widely spaced exploration drill holes. The data base for the upper orebodies is a better sample: the upper orebodies were drilled over their full areal extent on a semiregular 25- to 50-m development grid. The Upper Yampa orebody data presented here include only drilling east of the East fault. The Upper Parnell orebody data include composites from five drill hole intersections in the steep limb of the syncline just to the southwest of the syncline axis. The spatial data configuration is shown projected on plan (Fig. 7). The Upper Parnell orebody was selected for more detailed structural analysis because it is the major host for high-grade gold mineralization.

Equal-length (1.5 m) composites of assays for each drill hole intersecting the orebodies in the northeast limb of the Bingham syncline were used to generate the grade histograms for copper (Fig. 8A and B) and gold (Fig. 9A and B), plotted to a log scale. Copper-grade histograms appear to approximate lognormal

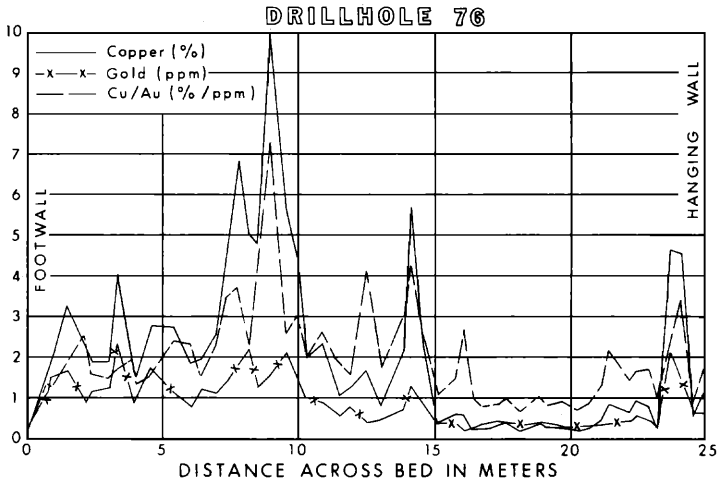

FIG. 6. Assay values for copper, gold, and the Cu/Au ratio across the Parnell limestone bed in a typical drill hole.

distributions except for the Lower Yampa orebody. The number of composites for the Lower Yampa (N = 83) is small and the composites have less even spatial distribution; both factors could explain the apparent bimodal distribution. Both the Upper and Lower Yampa orebodies are considerably richer in copper than the Parnell.

The gold-grade histograms also appear to approximate lognormal distributions. The apparent bimodality of the lower orebody gold distributions, i.e., the low tail of the distribution, is caused by the assay detection limit cutoff. This also explains the high coefficient of variation (C.V.) for the lower orebodies.

Experimental mean gold grade (m) in the upper orebodies (0.7 ppm) is higher than in the lower orebodies (0.3 ppm). The elevation range represented by the lower orebodies is 450 to 1,100 m, and for the upper orebodies, 1,100 to 1,400 m. The average grade of gold in the near-surface (approximately 2,000-m elevation) skarns was in the range 0.15 to 1.5 ppm gold, using Boutwell's (1905) figures.

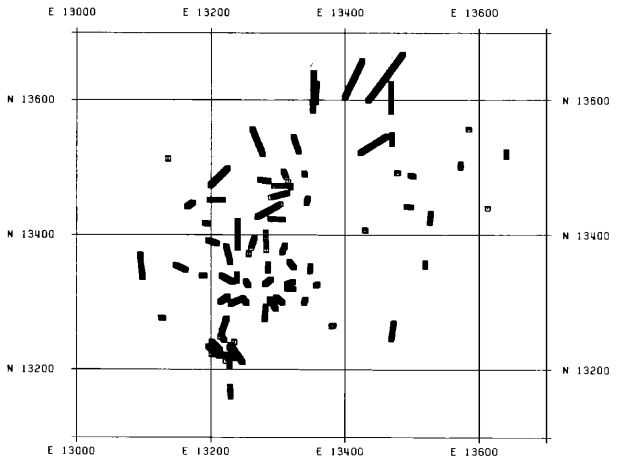

FIG. 7. Drill hole composite locations for the Upper Parnell orebody projected to plan view.

Scatterplots for copper and gold for each orebody (Fig. 10A–D) show that copper and gold are correlated. The correlation coefficients (r), experimental mean Cu/Au ratios for each bed, and experimental mean copper and gold values are given in Table 2.

Some intermingling of a second, high-grade gold mineralization (discussed below) is the cause of the greater scatter in the Upper Parnell orebody scattergram (Fig. 10D), and the lower correlation coefficient for copper and gold. Table 2 and the scattergrams both show that the Cu/Au ratio decreases in the upper orebodies. The Parnell orebodies also have a higher gold content relative to copper than do the Yampa orebodies.

The Cu/Au ratio varies across the width of each bed as well (e.g., Fig. 6), being generally higher near the footwall and hanging wall and lowest near the upper half to third of the bed. Higher Cu/Au ratios and copper grades at the edges of the beds may occur because some mineralization pulses were more copper rich than others. Most of the textural evidence of multiple copper mineralization pulses, described above, is observed near the contacts of the skarn beds.

Atkinson and Einaudi (1978, p. 1357) suggested that whole-bed copper grades vary with distance from the Bingham quartz monzonite porphyry stock contact, which at depth strikes approximately N 40° E. Whole-bed-grade contours constructed from all of the Upper Parnell orebody exploration and development drilling (Fig. 11) indeed show a range in strike from N 20° E to N 50° E.

Semivariograms are a statistical device used to show characteristics of the spatial variation between sample grades within a statistical population as a function of

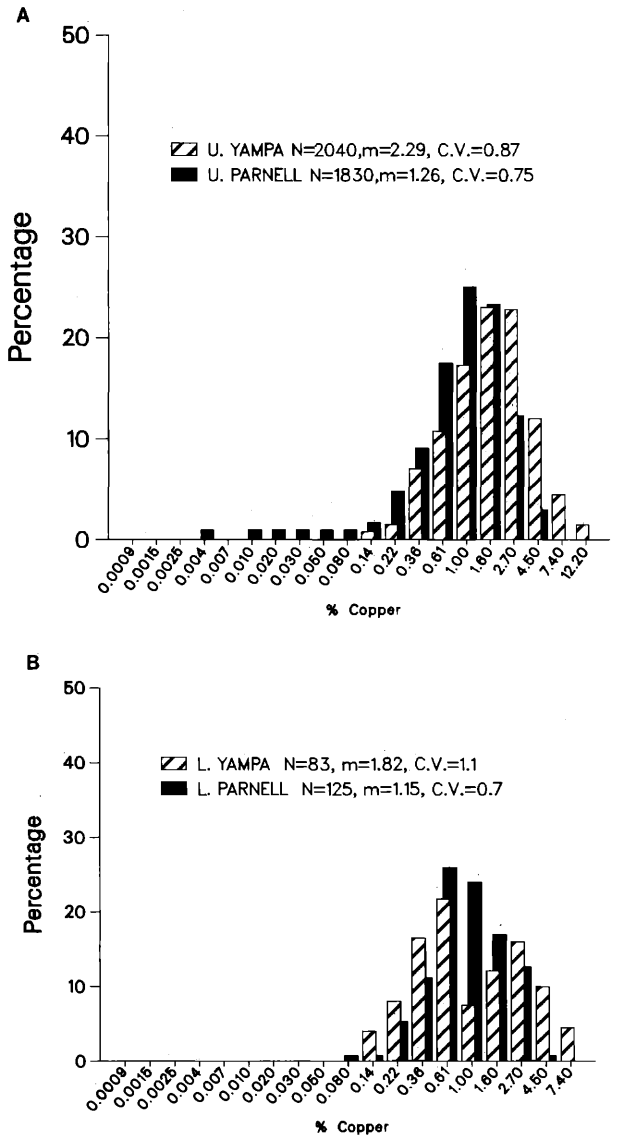

FIG. 8. Copper histograms of drill hole composites for Lower (A) and Upper (B) orebodies, N = number of composites, m = experimental mean, C.V. = coefficient of variation. Log scale.

distance in a given direction. In many base metal deposits the variogram value will increase with distance up to a certain distance, called the range, beyond which grades are uncorrelated. The value of the variogram beyond which there is no increase is called the sill value. Directional copper-grade variograms for the Upper Parnell orebody constructed in the plane of the bed are isotropic and reach a sill at a distance of approximately 60 m (e.g., Fig. 12A). The drift effect (e.g., Journel and Huijbregts, 1978, p. 313–315) arises from an inhomogeneity of the mineralization over a data field, e.g., from gradients in the grade. Copper mineralization shows a drift effect beyond 120 m in the 110° azimuth reflected in a rapidly increasing variogram slope. This direction is nearly perpendicular to the average strike of the stock contact and thus supports the hypothesis that distance to the stock is an important factor in the copper grade. Drift is also apparent at 175 m in the 20° azimuth and at intermediate distances in the variograms of intermediate azimuths.

The variograms may show a second control on copper grade acting in concert with the primary control, i.e., distance to the stock. The drift effect is least in the 20° azimuth, parallel to the N 20° E fault system, whereas the stock contact averages N 40° E. The

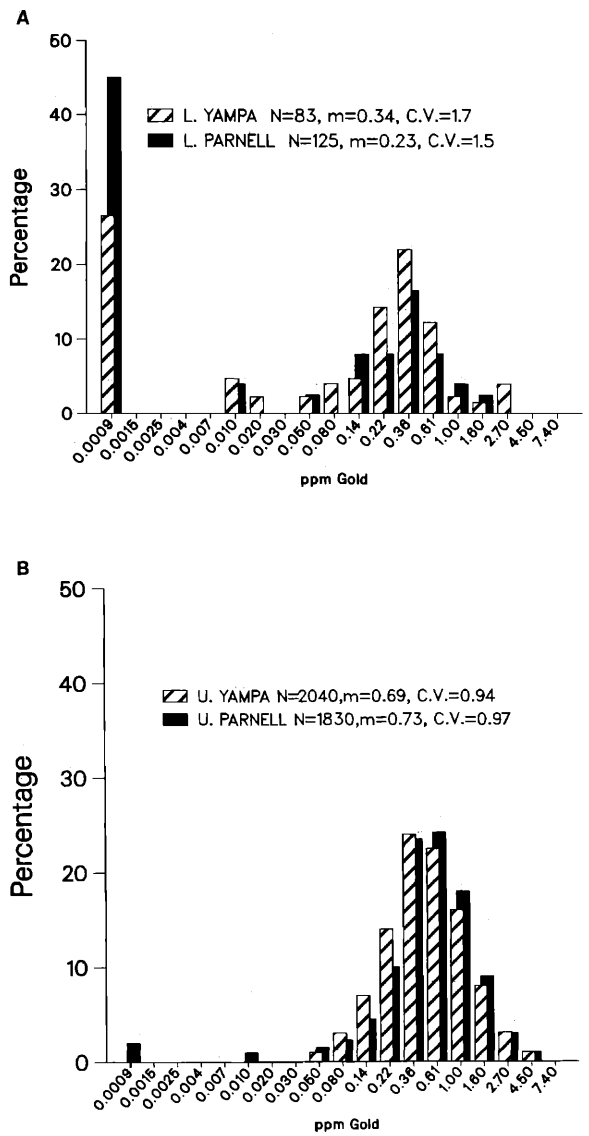

FIG. 9. Gold histograms of drill hole composites in the copper-gold mineralization: Lower (A) and Upper (B) orebodies. Log scale.

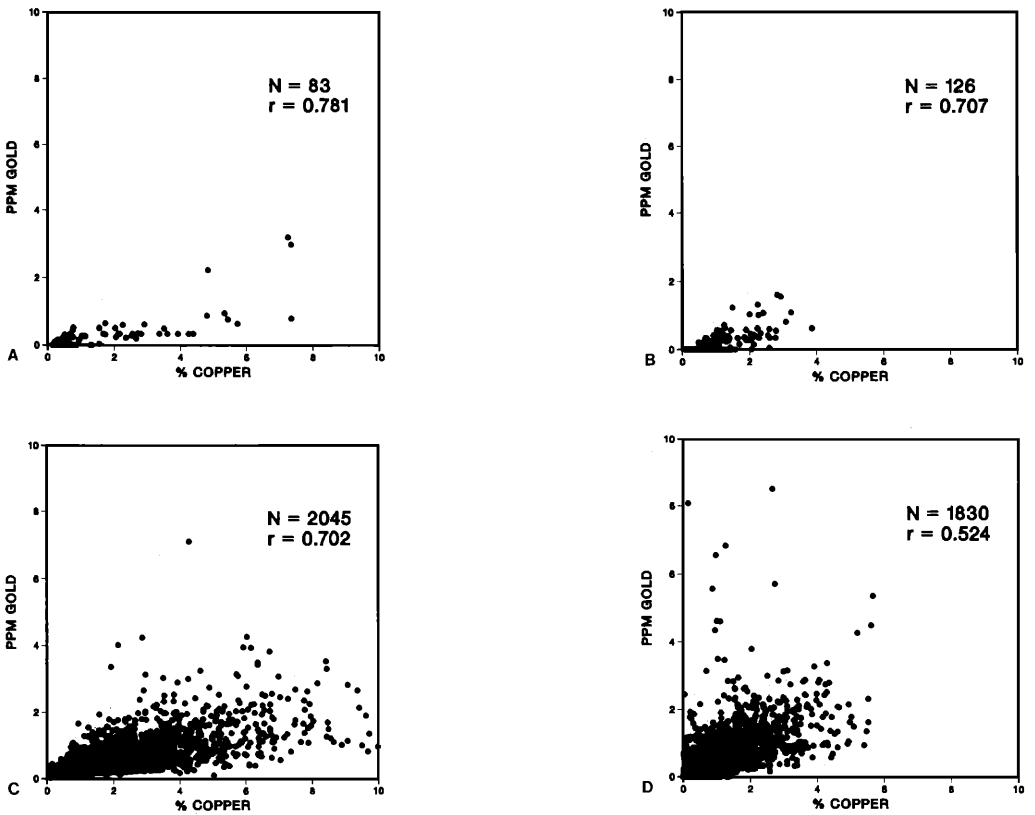

FIG. 10. Scatterplots of composited drill hole data for the gold-copper mineralization. (A) Lower Yampa, (B) Lower Parnell, (C) Upper Yampa, (D) Upper Parnell orebodies.

copper variograms thus complement geologic observations that the N 20° E faults were a major component of the hydrothermal plumbing system. The faults are major controls of fissure mineralization at higher levels in the district (e.g., Rubright and Hart, 1968, p. 895).

The variogram perpendicular to the dip of the Parnell limestone (Fig. 12A) quantifies the great variation in grade at short range (cf. the drill hole profile in Fig. 6) and suggests that the nugget is 0.1 percent copper.

The principal directions for gold variograms (Fig. 12B) appear to have the same orientation as copper variograms and show a drift effect at 125 m. The 20° azimuth variogram increases sharply and then maintains a gentle positive slope. The variogram appears

TABLE 2. Univariate Statistics for the Copper-Gold Orebodies

Orebody	n[1]	Mean Au (ppm)	Mean Cu (%)	r^2	Cu/Au (%/ppm)
Lower Yampa	83	0.34	1.82	0.781	5.35
Lower Parnell	126	0.23	1.15	0.707	5.00
Upper Yampa	2,040	0.69	2.29	0.702	3.32
Upper Parnell	1,830	0.73	1.26	0.524	1.72

[1] Number of composites in calculation
[2] Correlation coefficient for copper and gold

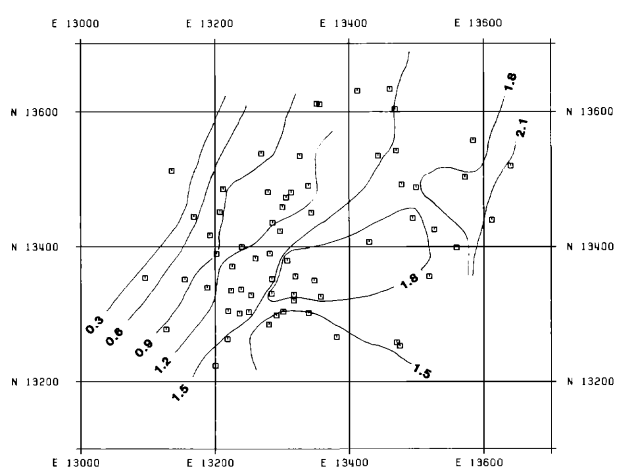

FIG. 11. Copper-grade contours in percent from drill hole whole-bed averages in the Upper Parnell orebody. Data points shown are midpoints of drill hole bed intercepts projected to horizontal plane.

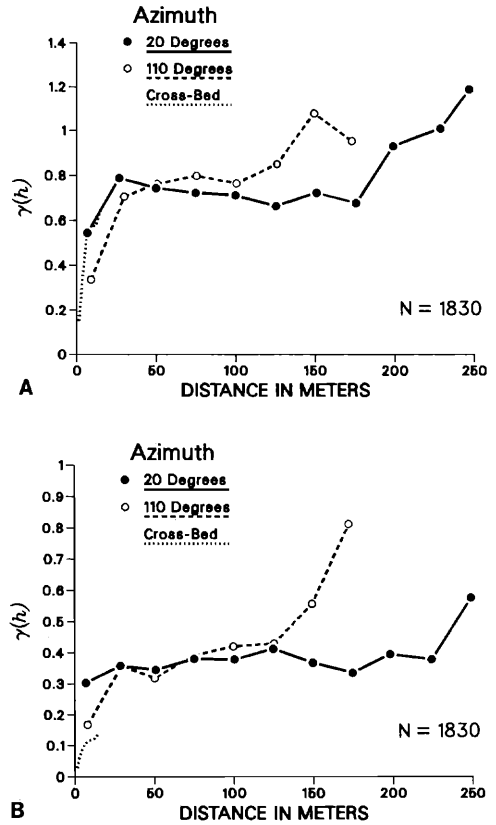

FIG. 12. Directional variograms for Upper Parnell drill hole composites: (A) copper, (B) gold. The total width of the data field in each direction shown is twice as large as the maximum experimental distance plotted.

to reflect perhaps two structures in the mineralization; the first with a range of approximately 30 m and the second with a range of approximately 100 m. The geologic significance of the two structures is unclear.

High-Grade Gold Mineralization

High-grade gold mineralization occurs locally in both the Yampa and Parnell orebodies and forms a continuous shoot traceable for several hundred meters in the Parnell orebody. The occurrence is separable from the copper-gold mineralization by geology, geochemistry, and geostatistics. The extent, the ultimate grade, and many other details of the gold mineralization are still unknown, but the gold occurrence is intriguing and may eventually be classified as gold ore.

General geology

Gold mineralization, first described by Atkinson and Einaudi (1978, p. 1359), occurs with fine-grained sulfides and clay or quartz alteration. The mineralization replaces gouge in minor northeast normal faults and joints. The altered and mineralized shears are generally cut by thin postmineral gouges. The limestone skarns host most of the gold mineralization, but all sedimentary rock types are locally mineralized.

The quartz-rich phase of the alteration-mineralization is dark gray and is easily recognizable in drill core and underground workings where it was mapped as "pyrite-quartz flood." Pyrite-quartz flood comprises quartz and fine-grained pyrite, with local coarse-grained pyrite, chalcopyrite, tennantite or tetrahedrite, and siderite. Pyrite may comprise up to 50 percent of some specimens; others are more quartz rich. Quartz lines vugs and has a pale blue cast in the quartz-rich samples. Most of the high gold assays are associated with pyrite-quartz flood alteration-mineralization. This mineralization replaced skarn wall rock locally and formed irregular fault-controlled pods in sharp contact with the copper-gold ores. Garnet appears to have been readily altered to siderite, quartz, and pyrite, but diopside appears to have been less readily altered and is often present as remnants enclosed in pyrite-quartz, and partially altered to an unknown clay mineral.

Fine-grained pyrite-clay occurring as similar fracture fillings has a much more widespread occurrence than the pyrite-quartz flood but is less visually distinct. Drill hole logs and workings maps did not always record the alteration or attempt to distinguish it from the pervasive montmorillonoid (saponite) alteration described by Atkinson and Einaudi (1978, p. 1359). Systematic arsenic assaying differentiated the two clay types. High levels of arsenic are always associated either with pyrite-quartz flood or pyrite-clay. Nothing is presently known of the clay mineralogy and chemical composition. The pyrite-clay alteration is not often in direct contact with the pyrite-quartz mineralization but often occurs in close spatial association with pyrite-quartz flood in drill hole intercepts.

Petrography of pyrite-quartz mineralization

The pyrite-quartz mineralization is divided into three stages based on detailed core logging and examination of approximately 50 polished ore sections and polished thin sections. Selected sections and minerals from intervals having high-grade gold assays were subsequently analyzed with the University of Wisconsin, Madison, ARL electron microprobe.

Stage 1 comprised flooding of the existing calc-silicate mineral assemblage by fine-grained quartz and pyrite (1-20 μ). The pyrite has a bronzy color on freshly broken or sawn surfaces. In polished section, stage 1 pyrite is pitted and appears to be intergrown with quartz gangue. Much of the pyrite is euhedral and occurs either as cubes or pyritohedrons. The pyrite/quartz ratio varies greatly from section to section, but bad plucking and polish in most of the sections (due to the hardness contrast of the minerals present) makes a quantitative estimate impossible. The pyrite/quartz ratio was approximately 1:1 in one bulk met-

allurgical sample (Norrgran et al., 1983). Table 3 lists partial chemical analyses of three stage 1 pyrites from a single polished section.

All three pyrites contain abundant arsenic. The gold content reported for analysis 3 may not be significant because considerable time elapsed between standard runs during the analysis. Abundant fine-grained disseminated arsenopyrite is present in one polished thin section. In another, pyrite appears to be pseudomorphous after specular hematite. It is not clear whether the hematite is relict from Main Stage copper skarn mineralization or whether it was introduced during an early stage of gold mineralization. Numerous stringers of quartz less than 1 mm in diameter with very minor sulfides cut much of the stage 1 pyrite-quartz flooding and may belong to one of the later stages.

Stage 2 mineralization comprises stringers of coarse pyrite and quartz which cut the stage 1 mineralization. Some of the large pyrite crystals have quartz cores. Magnetite is locally present as inclusions in large pyrite crystals or in various degrees of replacement by the pyrite crystals. The paragenetic relations suggest that an early quartz-magnetite assemblage in the veins was sulfidized later in the alteration. Stage 2 may thus reflect more than one mineralization event. Chalcopyrite, pyrrhotite, and arsenopyrite, remnants from earlier mineralization, were also identified as inclusions in stage 2 pyrites (e.g., Figs. 13 and 14). Some of the stage 2 stringers contain extensive intergrowths of fine-grained subhedral pyrite and quartz. Table 4 lists analyses of stage 2 pyrites from three polished sections representing different areas in the Upper Parnell gold shoot. Stage 2 pyrites contain significantly less arsenic than do stage 1 pyrites. Analysis 1 (Table 4) was made on a large subhedral pyrite crystal. The other analyses are of pyrite crystals coexisting with tennantite of stage 3, described below.

Stage 3 mineralization comprises fine-grained to very fine grained intergrowths of tennantite-tetrahedrite, pyrite, and locally chalcopyrite, shown in Figure 15A and B. Stage 3 mineralization is not evident in many of the drill hole intercepts. Tennantite may simply be replacing quartz gangue in the stage 2 pyrite-quartz intergrowths in some areas, but in others pyrite seems to have been replaced and/or recrystallized from coarse crystals into a pyrite-tennantite intergrowth. The evidence for replacement is that tennantite locally forms selvages on coarse-grained stage 2 pyrite crystals.

Chalcopyrite is locally associated with tennantite, especially as mantles or rims, or as microscopic-scale stringers. Microscopic textures indicate that tennantite did not replace chalcopyrite, but chalcopyrite is generally less abundant in pyrite-quartz flood than in the surrounding skarn. Atkinson and Einaudi (1978) observed that copper grades generally are very similar

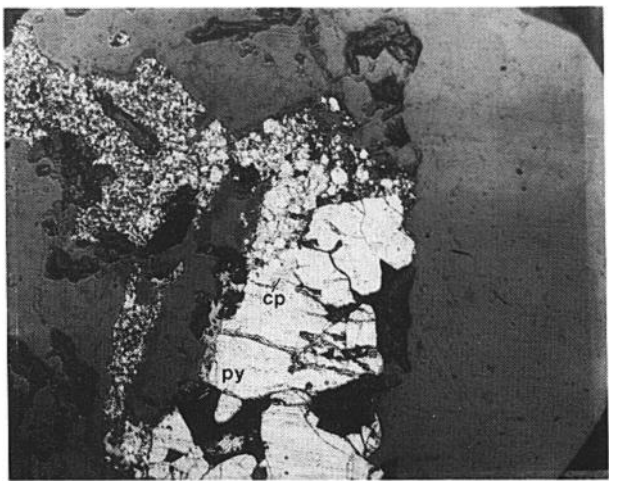

FIG. 13. Photomicrograph of inclusion of chalcopyrite in stage 2 pyrite. × 335.

TABLE 3. Electron Microprobe Analyses of Stage 1 Pyrites

	1	2	3
Cu	0.38	0.47	0.05
S	47.00	47.92	50.94
Fe	42.63	43.39	45.72
As	8.50	8.36	3.53
Sb	0.01	n.d.	0.01
Ag	n.d.	n.d.	n.d.
Au	n.d.	n.d.	0.03
Total	98.52	100.14	100.28

n.d. = not detected

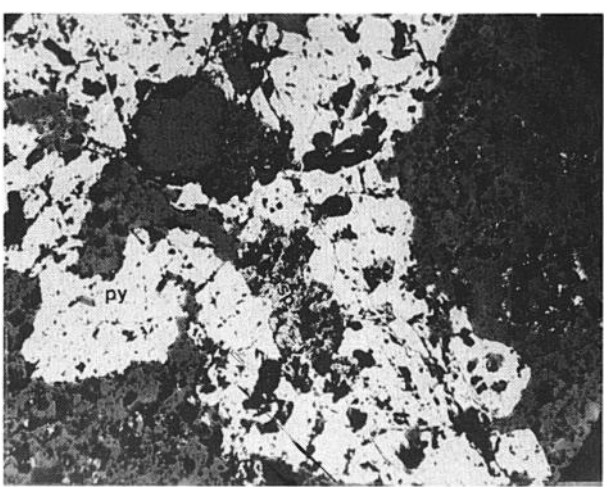

FIG. 14. Photomicrograph of arsenopyrite crystal in stage 2 pyrite. ×335.

TABLE 4. Electron Microprobe Analyses of Stage 2 Pyrites

	1	2	3	4	5	6	7
Cu	0.25	0.61	0.30	0.42	0.09	0.10	0.02
S	52.55	52.21	53.15	53.47	53.55	53.45	54.05
Fe	46.10	45.90	46.60	46.47	46.66	46.03	46.21
As	0.04	1.35	0.24	0.31	0.10	0.11	0.06
Sb	n.d.	n.d.	n.d.	n.d.	n.d.	n.d.	n.d.
Ag	n.d.	n.d.	n.d.	n.d.	n.d.	n.d.	n.d.
Au	n.d.	n.d.	n.d.	n.d.	n.d.	0.03	n.d.
Total	98.94	100.07	100.29	100.67	100.40	99.72	100.34

n.d. = not defected

in pyrite-quartz flood intervals and in the surrounding skarn.

Interesting sunburst textures resulted where tennantite replaced quartz in the quartz-pyrite intergrowths or filled voids in the centers of large subhedral pyrite crystals. Tennantite appears to have replaced the enclosing pyrite along radiating fractures in the crystals. Photomicrographs of the sunbursts are

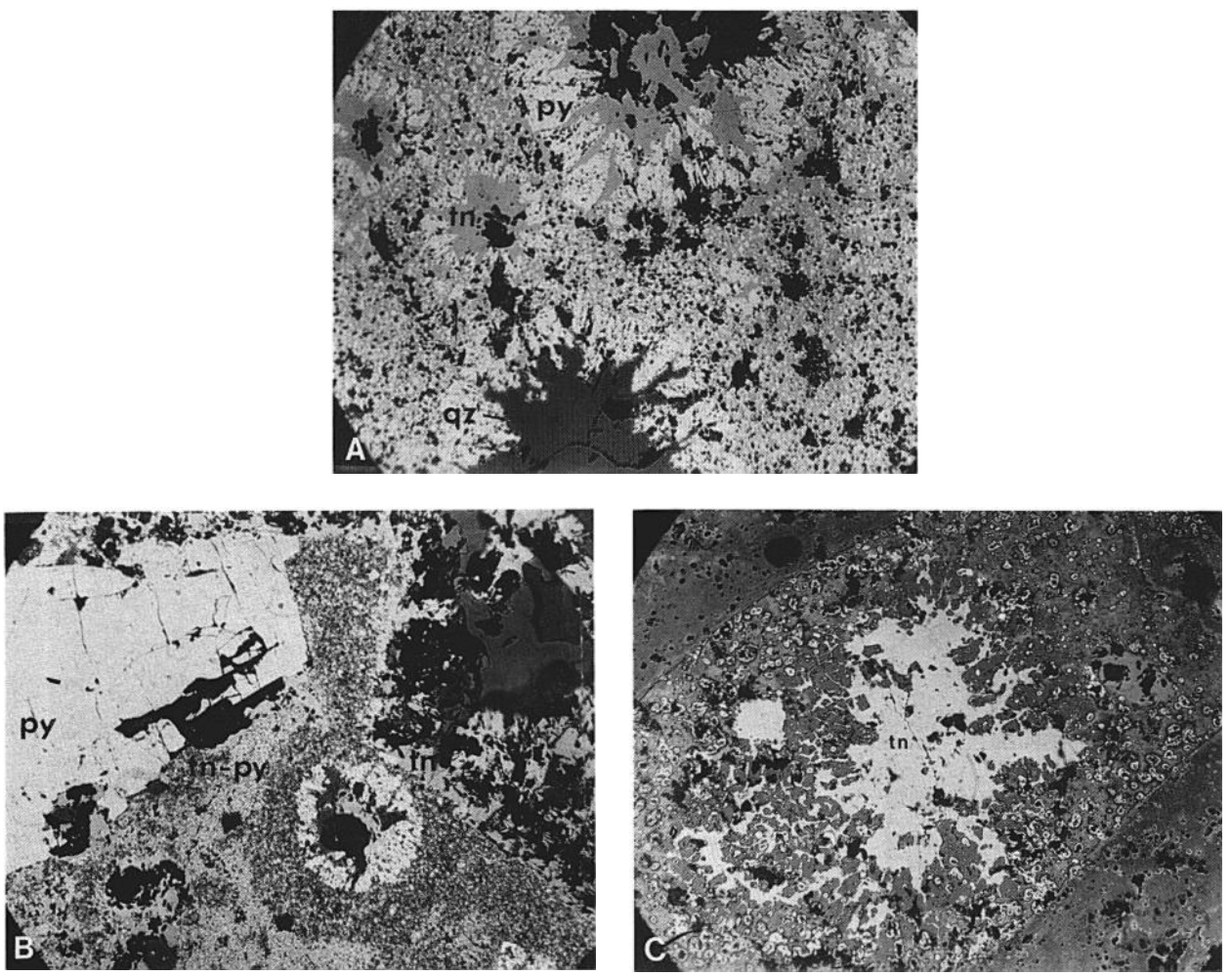

FIG. 15. Photomicrographs of tennantite-pyrite intergrowths. A. Matrix of tennantite-pyrite with portions of sunbursts. B. Large stage 2 pyrite in matrix of tennantite-pyrite, sunburst, and coarse tennantite (right-hand side). C. Detail of sunburst. All ×175.

TABLE 5. Electron Microprobe Analyses of Tennantite-Tetrahedrite

	1	2	3	4	5	6	7
Cu	42.74	42.54	41.94	43.14	42.73	37.73	38.75
S	28.64	28.80	28.61	28.96	28.86	25.08	25.79
Fe	6.68	7.46	8.02	6.81	7.47	2.95	3.32
As	19.65	19.52	19.41	20.20	19.98	5.87	7.71
Sb	0.60	0.54	0.28	n.d.	n.d.	20.91	18.57
Ag	0.05	n.d.	n.d.	n.d.	n.d.	0.13	0.14
Au	n.d.	n.d.	n.d.	n.d.	n.d.	n.d.	n.d.
Zn						4.45	4.07
Total	98.36	98.86	98.26	99.11	99.04	97.12	98.35

n.d. = not defected

shown in Figure 15. In drill cores tennantite in quartz veins is locally visible with the unaided eye where it formed anhedral crystal aggregates and massive replacements, some with chalcopyrite. Table 5 reports partial electron microprobe spot analyses of tennantite-tetrahedrite grains from three polished sections.

Tennantites associated with pyrites in sunbursts (Tables 5, analyses 1, 2, 3, and 5) and the tennantite from a pyrite-tennantite matrix intergrowth (analysis 4) contain only traces of antimony and silver. Analyses 6 and 7 are tetrahedrite-tennantite with high zinc. Both of the tetrahedrites are intergrown with chalcopyrite. The ratio As/Sb varies significantly within single crystals.

Trace amounts of gold reported in some of the analyses may not be significant because of spectrometer drift. Metallurgical testing of quartz-pyrite mineralization by Norrgran et al. (1983) suggests that the gold is contained as submicroscopic inclusions in pyrite. Most of the drill hole intercepts which contained tennantite also had high gold assays. Efforts in this study to locate gold grains in polished sections and with a widened electron beam were not successful.

Paragenetic sequence of mineralization

The first mineralization at Carr Fork comprised copper-gold mineralization of garnet-diopside skarn, perhaps in several pulses. Megascopic observations show that high-grade gold mineralization followed formation of copper-gold orebodies. The gold-bearing mineralization, comprising widespread pyrite-clay and pyrite-quartz flood, occurred in three stages. Wall-rock replacement by predominantly quartz and arsenical pyrite composed stage 1. Crosscutting stringers of quartz containing coarse pyrite and quartz-pyrite intergrowths composed stage 2. Tennantite or tetrahedrite with subordinate chalcopyrite replaced the quartz gangue locally (stage 3). Some chalcopyrite stringers cut stage 3 pyrite-quartz mineralization. Quartz-molybdenum veins always cut pyrite-quartz mineralization and appear to be the last recorded hydrothermal event.

Univariate and spatial distribution of gold

Equal-length (1.5 m) composites of pyrite-quartz mineralization compose a bimodal histogram, shown on log scale in Figure 16. All of the composites are from the Upper Parnell and Steep Parnell copper-gold orebodies, and nearly all are from the Parnell gold shoot, described below. The modes of the histogram are the 0.61-ppm-grade class and the 12.2-ppm-grade class. The histogram appears to reflect two populations: a low-grade gold mineralization corresponding to the copper-gold skarn event, and a separate high-grade gold mineralization. The scattergram for gold and copper in pyrite-quartz flood (Fig. 17) contrasts sharply with the gold-copper scattergram for the Upper Parnell orebody (Fig. 10D). The value for the correlation coefficient for gold and copper, −0.093, shows that they are uncorrelated in pyrite-quartz mineralization. The coefficient of variation (standard deviation divided by the mean), 1.07, is fairly low for gold mineralization compared to other

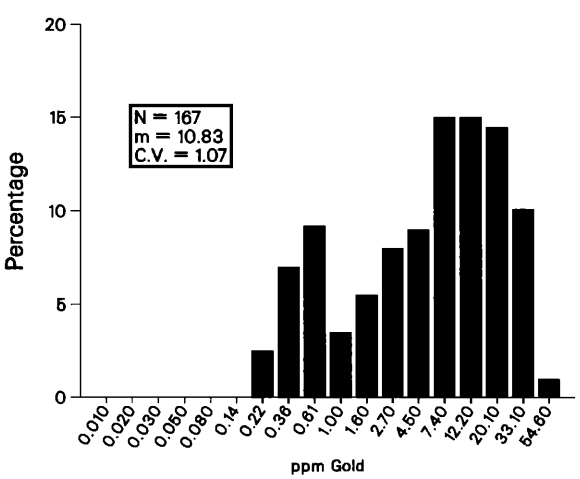

FIG. 16. Gold histogram of drill hole composites for pyrite-quartz mineralization plotted to log scale.

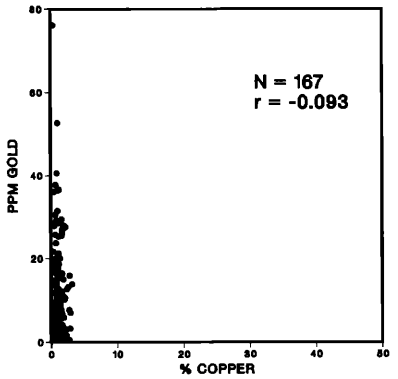

FIG. 17. Scatterplot of drill hole composites for the pyrite-quartz flood mineralization.

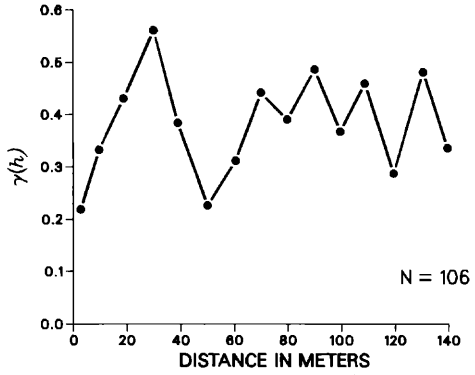

FIG. 18. Directional variogram (20° azimuth) for log-transformed gold grade oriented along the long axis of the Parnell gold shoot. The total width of the data field is twice as large as the maximum experimental distance plotted.

known deposits and reflects the wide spread and high mean of the distribution.

The variogram for gold grade calculated in the direction of the long axis of the gold shoot (described below) increases rapidly within a short distance but then becomes very erratic. The number of pairs at each lag of the variogram also drops from more than 100 pairs up to 25 m to much less than 100 pairs beyond 25 m. Outlier grades as high as 76 ppm gold distort the grade variogram.

Transformed grades sometimes produce variograms which show a clearer spatial structure for mineralization. However, the variogram for the log transform of gold grade (Fig. 18) and indicator variograms (cf. Journel, 1983) appear to show some reliable correlation between gold composites only up to approximately 20 m. The variogram of log of grade includes only composites with values greater than 4.0 ppm gold in order to filter out the skarn gold component of the population. The addition of more composite data from future drill holes might improve the results.

Parnell gold shoot

Gold mineralization accumulated in a distinct shoot from 15 to 30 m wide centered on the Parnell skarn orebody immediately above workings of the Carr Fork mine. The shoot lies almost parallel to the East fault and approximately 20 to 50 m east of the fault. The perspective diagram (Fig. 3) offers an overall view of the shoot. The shoot formed at the intersection of a near-vertical en echelon fault and fracture zone with the Parnell limestone, and locally, the surrounding lithology as shown in Figure 4. The Bullard limestone, separated from the Parnell limestone by approximately 10 m of quartzite (not shown in Fig. 4), was also a favored host.

The root zone of the gold shoot is exposed in a single crosscut drift in quartzite. The drift is cut by a series of N 20° E en echelon faults with 2.5-m spacing. A thin marker bed in the crosscut demonstrates only

TABLE 6. Trace and Major Element Analyses

Sample	Au[3]	Cu[4]	Tl	Pt[3]	Pd[3]	Se	As	Sb	Hg	Cr	Ni	U	Th	W	Pb
1	0.028	1.5	ND	0.002	0.028	18	28	ND	0.05	66	22	12	7	26	27
2	0.014	4.7	ND	0.006	0.026	17	35	14	0.03	61	16	13	ND	85	67
3	0.006	0.79	ND	0.002	0.013	16	45	16	0.03	53	36	11	ND	46	36
4	0.770	1.1	23	0.008	0.008	ND	1.16[4]	971	5.10	190	105	13	ND	16	246
5	0.232	0.73	48	0.007	0.007	ND	1.95[4]	164	0.98	110	110	5	3	7	35
6	0.374	0.34	75	0.010	0.005	ND	2.98[4]	233	0.52	100	46	7	13	5	23
7	0.274	0.22	55	0.003	0.003	6	2.54[4]	192	0.78	5	25	4	ND	22	71
8	0.930	0.02	28	0.002	0.004	7	1.66[4]	49	0.17	38	13	8	ND	55	42
9	0.092	0.81	160	0.007	0.007	ND	0.74[4]	154	2.00	120	120	9	3	40	139

[1] All analyses by Anaconda Research in Tucson, except U and Th (Skyline Labs, Inc.)
[2] Analyses reported in ppm except as noted
[3] Fire assay in oz/short ton
[4] Analysis in percent
ND = not deleted

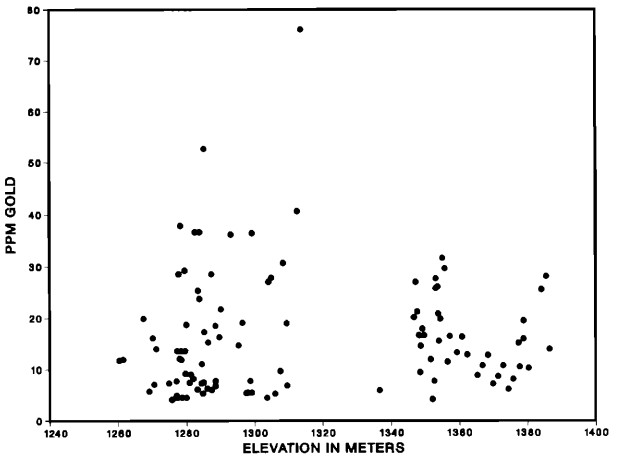

FIG. 19. Pyrite-quartz flood composite gold grades versus elevation at a 4.0 ppm cutoff. The lower part of the gold distribution has been truncated to show trends in the high-grade population.

minor offset along the faults. Pyrite-quartz flood and pyrite-clay mineralization bearing high arsenic and gold values fills several of the faults and locally has flooded outward in narrow replacement zones in the wall rock.

Drill hole intercepts of the Parnell gold shoot comprise intervals of Main Stage copper-gold skarn interspersed with narrow (0.1–3.0 m) intervals of pyrite-quartz mineralization. Much of the clay-pyrite mineralization is probably lost in the drilling process. It is not presently known whether individual pods or small shoots can be followed within the larger shoot.

The present drill-indicated geologic resource for the Parnell gold shoot from cross sections is 800,000 metric tons of 1.02 percent copper, 8.73 ppm (0.255 troy oz/short ton) silver, and 4.20 ppm (0.122 troy oz/short ton) gold. Inferred reserves in areas of lower drilling density include an additional 400,000 tons. The resource is significantly diluted with copper-gold skarn ore and does not include mineralization that exists outside of the Parnell bed. Most of the resource is in the Upper Parnell copper-gold orebody (cf. Fig. 3), where it has been followed by drilling from the axis of the Bingham syncline northward 200 m. The resource also includes mineralization that continues south of the fold axis in the steep limb of the syncline. This part of the shoot is known from core drilling to extend upward at least 100 m in the Parnell limestone skarns to the 1,400-m level. The shoot is open-ended updip in the steep limb and northward in the gently dipping limb of the syncline, at least to the Parnell intersection with the Markham fault. Figure 19, a plot of grade of the drill hole 1.5-m composites versus elevation, shows no clear trend. The gap in the data reflects a lack of drilling information in the interval 1,310- to 1,350-m elevation.

Other gold mineralization is scattered widely throughout the other orebodies, including an exposure in the Yampa orebody from the deepest level of the mine, the 970-m level. Thus, the mineralization occurs sporadically within a vertical interval of at least 450 m. The mine exposures of pyrite-quartz flood in the skarn are in northeast-striking faults. Known occurrences of pyrite-quartz flood outside of the Parnell shoot are not traceable over significant lengths nor are they more than 1 m in width. Curiously, neither anomalous gold nor arsenic is present in drill holes intersecting Yampa limestone skarns beneath the Parnell gold shoot.

Comparison of Trace and Major Elements

Trace and major elements strongly differentiate the copper-gold ores and the pyrite-quartz flood gold mineralization. The data include three copper-gold

from the Yampa and Parnell Limestone Beds[1,2]

Zn	Mo	Co	Mn[4]	Ag[3]	F[4]	Cd	Bi	Sn	Sr	Ba	Te	S	SiO_2[4]	CaO[4]	Fe[4]
150	90	36	0.13	0.28	0.075	ND	18	15	ND	19	ND	8.5	37.4	18.0	16
102	70	15	0.14	ND	0.090	ND	ND	12	17	ND	ND	1.6	44.3	20.9	12
130	135	27	0.13	0.18	0.120	ND	ND	15	19	199	ND	6.5	45.7	15.0	13
630	48	31	0.06	0.24	0.100	ND	ND	4	5	ND	ND	13.3	65.3	1.16	12
150	51	25	0.19	0.30	0.070	ND	6	9	6	15	ND	15.8	54.5	2.68	15
115	120	24	0.17	ND	0.083	ND	ND	7	5	19	ND	16.3	50.0	2.82	14
35	8	4	0.54	ND	0.054	ND	ND	8	15	ND	ND	21.3	26.3	11.7	16
15	20	12	0.09	0.32	0.062	ND	ND	8	7	ND	ND	24.4	29.9	6.4	19
310	50	37	0.16	0.22	0.160	ND	ND	6	22	47	ND	7.5	61.2	5.4	8

Sample locations: 1 = Parnell skarn east of gold zone; 2 = Parnell skarn west of East fault and gold zone; 3 = Parnell garnet skarn in and near gold zone but without quartz-pyrite mineralization; 4 = gold zone ore in Steep Parnell; 5 = gold zone ore, central location, Upper Parnell orebody; 6 = gold zone ore, north end of known mineralization in Upper Parnell orebody; 7 = Yampa pyrite-quartz mineralization from 970-m level; 8 = Yampa pyrite-quartz mineralization from 1,155-m level, 1,155–1,080 vent raise access; 9 = Yampa pyrite-quartz mineralization from 1,200-m level

skarn samples from different areas of the Upper Parnell skarn orebody. Each sample contained equal amounts of material from the footwall, center, and hanging-wall parts of the bed, and comprised material from several drill holes. Care was taken to avoid intervals containing abundant Late Stage clay alteration. Likewise, three composite samples of pyrite-quartz mineralization were selected from different areas of the Parnell gold shoot. Another three samples of Yampa pyrite-quartz mineralization from the Steep Yampa skarn orebody complete a wide range of elevation and lateral distance for the comparison.

Table 6 presents analytical results for skarn (samples 1–3) compared with the selected pyrite-quartz flood samples (samples 4–9). The table is arranged into three groups of elements from left to right: trace and minor elements showing obvious differences between skarn and pyrite-quartz flood; those showing no obvious differences; and major elements. Analytical results and individual sample descriptions are shown in Table 6. The pyrite-quartz flood gold mineralization is enriched in thallium, arsenic, antimony, mercury, sulfur, and silica relative to the skarn ores. Arsenic, mercury, sulfur, and silica represent significant additions to the bulk chemistry. The mercury-bearing phase is not known but might be tennantite. Arsenic is the most strongly enriched element and is known to be widespread in the argillic phase of the gold mineralization. The gold shoot samples show apparent enrichment in chromium and nickel; the samples contain abundant quartz and were probably contaminated by the crusher and pulverizer liners.

Pyrite-quartz flood is depleted in palladium, selenium, and calcium relative to skarn ore. The palladium values in the Parnell skarns are significant and have not been reported previously. Trace and major element differences in pyrite-quartz mineralization are not apparent between the Yampa and Parnell limestone beds nor is there a gradient with respect to elevation.

Molybdenum values in skarn and pyrite-quartz flood are similar enough to confirm megascopic observations that quartz-molybdenum veins cut the pyrite-quartz flood. Pyrite-quartz flood is thus an intermineral event between copper-gold and molybdenum rather than the latest event in the evolution of the porphyry system.

Conclusions

Geologic mapping, petrography, univariate statistical analysis, and geochemistry distinguish two gold-bearing mineralization events in the Carr Fork orebodies. The gold-copper mineralization reflects three major grade controls: (1) the quartz monzonite porphyry contact, (2) host rock, and (3) a northeast-trending fault set. Copper-gold mineralization formed orebodies in limestone skarn arrayed within a range of distances from the porphyry contact. Mineralizing solutions entered the beds along the northeast fault set. Elevation was perhaps an additional control on the skarn gold because the structurally lower orebodies have less gold than the upper orebodies.

The high-grade gold mineralization (pyrite-quartz flood) also appears to be localized by the northeast fault set and favorable host rock (skarn), but it does not reflect a clear relationship of distance to the stock nor to elevation. Drilling is not sufficient to determine whether high-grade gold mineralization is present in the lower orebodies. The Yampa and Parnell limestone skarns were both favorable hosts, but structural preparation of the Parnell skarn was apparently better in the gold shoot area.

The gold mineralization is widespread and is probably related to the emanation of hydrothermal solutions from an igneous source. The paragenetic sequence of mineralization; copper-gold, followed by gold, and finally molybdenum, has no close analogue in porphyry copper literature. Perhaps the gold mineralization emanated from a different igneous source rock within the Bingham stock.

The diluted geologic high-grade resource, 1.2 million metric tons, is small but significant. The undiluted grade of the pyrite-quartz mineralization might be approximately 10 to 12 ppm (0.3-0.35 oz/short ton gold), using as an estimate the experimental mean value of the histogram (cf. Fig. 16). The potential for extensions of the Parnell gold shoot and for enhancement of grade upward in the steep limb of the Bingham syncline is speculative. Certainly, gold occurs 600 m above the top of the drilled portion of the shoot with copper in the skarns. The data presented in this paper do not show any gradients in the grade, physical characteristics, or statistics of the gold event. Therefore, given a favorable structural environment, the shoot could well continue upward. Perhaps the gold shoot(s) grades upward into the lead-zinc fissure ores. Rubright and Hart (1968, p. 900) stated: "Erratic high-grade gold and silver were mined from some of the lead-zinc ore shoots on the lower levels (of the U. S., Utah metals, and other mines)." Lindgren (1933) described an ore shoot in the Leadville vein in the Carr Fork mine which graded downward into tennantite-chalcopyrite ore.

Preliminary metallurgical testing by Norrgran et al. (1983) demonstrated that the gold is refractory to leaching and cannot be adequately concentrated by flotation. High arsenic values associated with the ore would pose a smelting problem as well. However, new extractive technology, such as biological leaching, might make the gold target of economic interest. If so, other shoots might be found in or adjacent to the northeast faults elsewhere in the Bingham district, and Bingham might add a new ore type to an already impressive list.

Acknowledgments

The authors thank the Anaconda Minerals Company for generous financial support, use of the computer and graphics software, and permission to publish this material. The staff of Anaconda Research provided the rock chemical analyses. Everett Glover of the University of Wisconsin, Madison, assisted the senior author with the microprobe analyses. Eugene N. Cameron contributed greatly to the petrographic interpretation. Andre Journel of Stanford University provided patient instruction in geostatistics and a thoughtful reading of the manuscript. John Baker kept the authors on the right track with key observations and an unflagging interest in the study. The authors also wish to thank all of the geology staff at Carr Fork for their helpful suggestions and patience.

March 13, October 9, 1986

REFERENCES

Atkinson, W. W., Jr., and Einaudi, M. T., 1978, Skarn formation and mineralization in the contact aureole at Carr Fork, Bingham, Utah: ECON. GEOL., v. 73, p. 1326–1365.

Boutwell, J. M., 1905, Economic geology of the Bingham district, Utah: U. S. Geol. Survey Prof. Paper 38, p. 73–387.

Emmons, S. F., 1905, Introduction of general geology: U. S. Geol. Survey Prof. Paper 38, p. 19–25.

Hansen, L. A., 1961, The stratigraphy of the Carr Fork mines, Bingham mining district, Bingham, Utah: Utah Geol. Mineralog. Survey, Guidebook to the Geology of Utah, no. 16, p. 71–81.

Hunt, R. N., 1924, The ores in limestones at Bingham, Utah: Am. Inst. Mining Metall. Engineers Trans., v. 70, p. 856–883.

Journel, A. J., 1983, Non-parametric estimation of spatial distributions: Math. Geology, v. 15, p. 445–468.

Journel, A. J., and Huijbregts, C. J., 1978, Mining geostatistics: New York, Academic Press, p. 1–580.

Keith, A., 1905, A section on areal geology: U. S. Geol. Survey Prof. Paper 38, p. 29–72.

Lindgren, W., 1933, Mineral deposits, 3d ed.: New York, McGraw-Hill, 930 p.

Norrgran, D. A., Salek, H., and Milligan, D. A., 1983, Mineralogical and metallurgical examination of Carr Fork—Upper Yampa gold-bearing pyrite: Denver, Colorado, ARCO Coal, Anaconda Research unpub. rept. 83–29, p. 1–21.

Rubright, R. D., and Hart, O. J., 1968, Non-porphyry ores of the Bingham district, Utah, *in* Ridge, J. D., ed., Ore deposits of the United States, 1933–1967 (Graton-Sales vol.): New York, Am. Inst. Mining Metall. Petroleum Engineers, p. 886–908.